



**HAL**  
open science

# Origin of an unusual systematic variation in the heteroepitaxy of Ag on Ni-the roles of twinning and step alignment

P. Wynblatt, Dominique Chatain, A D Rollett, U. Dahmen

## ► To cite this version:

P. Wynblatt, Dominique Chatain, A D Rollett, U. Dahmen. Origin of an unusual systematic variation in the heteroepitaxy of Ag on Ni-the roles of twinning and step alignment. Acta Materialia, In press. hal-02002808v1

HAL Id: hal-02002808

<https://amu.hal.science/hal-02002808v1>

Submitted on 31 Jan 2019 (v1), last revised 14 Feb 2019 (v2)

**HAL** is a multi-disciplinary open access archive for the deposit and dissemination of scientific research documents, whether they are published or not. The documents may come from teaching and research institutions in France or abroad, or from public or private research centers.

L'archive ouverte pluridisciplinaire **HAL**, est destinée au dépôt et à la diffusion de documents scientifiques de niveau recherche, publiés ou non, émanant des établissements d'enseignement et de recherche français ou étrangers, des laboratoires publics ou privés.



Distributed under a Creative Commons Attribution 4.0 International License

# Origin of an unusual systematic variation in the heteroepitaxy of Ag on Ni – the roles of twinning and step alignment

P. Wynblatt<sup>1\*</sup>, D. Chatain<sup>2</sup>, A. D. Rollett<sup>1</sup>, U. Dahmen<sup>3</sup>

<sup>1</sup>Department of Materials Science and Engineering, Carnegie Mellon University, Pittsburgh PA 15213, USA

<sup>2</sup>Aix-Marseille Univ, CNRS, CINaM, Marseille, France

<sup>3</sup>NCEM-Molecular Foundry, LNBL, Berkeley, CA 94720, USA

## **ABSTRACT**

A systematic variation in the orientation relationship (OR) of Ag films grown on Ni substrates previously discovered by a combinatorial approach is analyzed using concepts of grain boundaries, surface science and phase transformations. On roughly half of all Ni substrate orientations, Ag adopts a “special” OR that varies systematically from a twin OR, which develops on substrates lying along the (111)-(210) line of the standard stereographic triangle (SST), to the so-called oct-cube OR, which arises exclusively on (100) substrates. On the other half of Ni substrate orientations, Ag adopts the standard cube-on-cube OR. The special ORs are modeled by a) linear interpolation, b) 1D edge-to-edge matching and c) 2D transformation strains, using the twin relationship as a reference. The 1D model shows that the systematic variation in the special ORs can be understood in terms of a growth mechanism by attachment at steps and a lattice rotation due to the difference between the step heights in the substrate and the film. The 2D model explains why this mechanism does not apply to substrates on which Ag displays the cube-on-cube OR.

**Keywords:** orientation relationship; combinatorial approach; epitaxial growth; twin; strain accommodation.

---

\* corresponding author

## **1. INTRODUCTION**

The orientation relationship (OR) that develops when a thin film is equilibrated on a single crystal substrate is essential to a fundamental understanding of the factors that control thin film growth and texture. A great deal of research has been devoted to understanding the structure and OR at the interface between film and substrate [1-3]. Most of the studies have been dedicated to a rationalization of the interfaces that develop between new phases/precipitates and their surrounding matrices during phase transformations [2,4]. These interfaces between different phases often develop as a result of phase separation such as martensitic transformations or precipitation reactions. Here, the major question is how the orientation and structure of the interface (or habit) plane, is determined by the need to accommodate the structural mismatch across the interface by lattice defects [1,5-10]. In phase transformations, the new phases are subjected to 3-dimensional (3D) constraints by being fully embedded in the matrix, and generally display a single OR with the matrix that must adapt to the orientations of all of its interfacial planes. This is different from the case of heteroepitaxy, of interest here, which addresses the OR of an A-film on a B-substrate of a given surface orientation (2D constraint). This may be thought of as an inverse problem: rather than finding the optimum interface for a given OR, the challenge is to find the optimum OR for a given interface.

Different ORs may develop when a film is equilibrated on substrates of different orientations. Such behavior was recently reported for Ag films grown on Ni substrates [11,12], but was not previously fully explained. The theories that have been developed to describe ORs in epitaxy have identified a set of variables (lattice parameters, elastic constants, interfacial energies, etc.), which drive the OR between two phases abutting at a hetero-interface. Most of the discussion has concentrated on the role of terraces, steps and defects (such as dislocations) to accommodate structural differences or lattice mismatch across the interface [5-9,13-15].

On the experimental side, most studies of epitaxy have been limited to the behavior displayed by films on single crystal substrates of low-index or vicinal orientations. However, the combinatorial approach [16] of using electron backscatter diffraction (EBSD) to make statistical measurements of A films on *polycrystalline* B substrates has greatly expanded the range of accessible substrate orientations (e.g. [11,17,18]).

In two recent studies, we have compared experimental determinations by EBSD of the ORs of Ag particles equilibrated on some two hundred different Ni substrate orientations [11] with ORs obtained by computer simulation on twelve distinct Ni substrate orientations [12]. The simulations were performed by molecular dynamics (MD) in conjunction with embedded atom method (EAM) potentials [19] and showed excellent agreement with the experimental results [11]. More recently, MD simulations for the same system have also explored the different ORs that develop under 2D vs. 3D constraints [20].

In this paper, we aim at providing an original physical explanation of the ORs adopted by Ag on Ni. We first summarize how the ORs of Ag films observed on an uncommonly large set of Ni orientations spanning the whole SST can be sorted primarily into two kinds, namely "special" and cube-on-cube. We then present an

analysis of the data by merging approaches used by the grain boundary and interface science communities, together with those used in phase transformations. Our analysis does not aim at giving a detailed description of the structure of each interface as found in [21] but rather at understanding the general trends. The physical outcome is surprisingly simple and powerful for a more general approach to heteroepitaxy.

## **2. PREVIOUS RESULTS**

We begin with a summary of previous results presented in refs [11,12]. The Ni surfaces on which the Ag ORs have been measured by EBSD are presented in Fig. 1, in the form of a standard stereographic triangle (SST) with corners at (100), (111) and (110), and (hkl) plane indices defined such that  $h \geq k$ ,  $k \geq l$ ,  $l \geq 0$ .

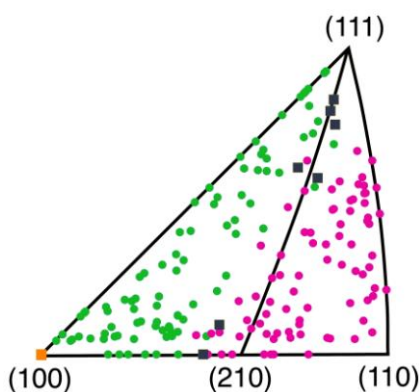


**Figure 1.** Standard stereographic triangle with poles of Ni(hkl) substrate surfaces [11] indicated by the points, and the measured ORs of the Ag film indicated by the colors of the points: pink = cube-on-cube, black = twin, orange = oct-cube, and green = "special" (see text). Notice the even distribution of Ni poles but the clear separation between the two major families of ORs (pink and green).

From the uniform distribution of Ni poles in Fig. 1 it is apparent that Ni substrate surface orientations were sampled fairly evenly across the entire orientation space. In contrast, the associated ORs of Ag on Ni, denoted by the colors of the symbols, are clearly divided into separate regions of the SST. The pink poles in the right segment indicate a cube-on-cube OR (*OR C*) in which the three cube axes of the Ag film are aligned with those of the Ni substrate. The green poles in the left segment represent a family of "special" ORs (*OR S*) which undergo a gradual but systematic transition between two delimiting ORs indicated by the orange square at the Ni(100) orientation (bottom left) and the central (111) to (210) dividing line located close to the set of black square symbols. The orange square indicates the oct-cube OR (*OR O*) which may be expressed as  $\text{Ag}(11\bar{1})[1\bar{1}0]//\text{Ni}(100)[0\bar{1}1]$ . The black squares indicate the twin OR (*OR T*), which may be written as  $\text{Ag}(111)[1\bar{1}0]//\text{Ni}(111)[0\bar{1}1]$ . Thus, orange, black and pink symbols denote three discrete ORs, whereas the family of green points (*OR S*) represents a continuous range of ORs stretching from the black points to the orange point, and which may be expressed as  $\text{Ag}(\text{HKL})[1\bar{1}0]//\text{Ni}(\text{hkl})[0\bar{1}1]$ . A major objective of this paper is to provide a connection between the two interfacial planes, Ag(HKL) and Ni(hkl), that form the observed

hetero-interface in the case of *OR S*. As far as the two parallel directions in the above description of *OR S* are concerned (i.e., Ag[1 $\bar{1}$ 0] and Ni[0 $\bar{1}$ 1]) the EBSD data analysis [11] has shown that these two <110> directions are those closest to lying within the interfacial plane.

One important point about the distribution of Ag interfacial planes that needs to be emphasized is that their orientations on all possible Ni substrate orientations are confined to just the (111)-(110)-(210) subtriangle of the SST. While it is obvious that for Ni substrates in the (111)-(110)-(210) subtriangle, where Ag adopts *OR C*, the orientation of Ag must also fall in that subtriangle, it turns out that on Ni substrates in the (100)-(111)-(210) subtriangle, where *OR S* prevails, Ag orientations are also confined to the same (111)-(110)-(210) region of orientation space. This rather striking and unexpected result for the ORs displayed by a relatively simple FCC-on-FCC heteroepitaxial system is in need of an interpretation. This explains our focus on relating the interfacial orientation of Ag(HKL) to that of Ni(hkl) in the region where *OR S* is observed, and to seek a rationale for the factors that may stabilize *OR C* in other regions of orientation space.

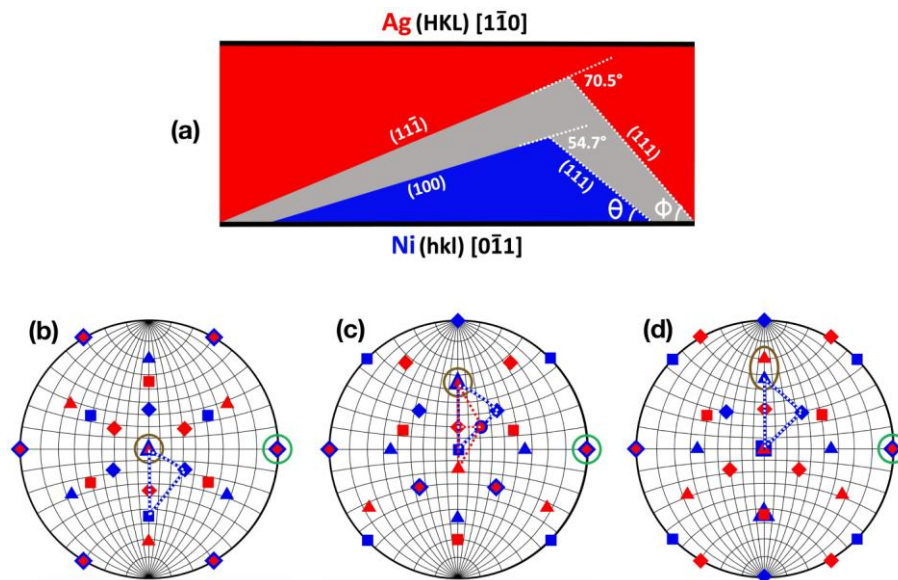


**Figure 2.** (a) Schematic of the OR of a Ag crystal on a Ni substrate lying along the (100)-(111) edge of the SST. Each crystal is viewed along a <110> axis (Ag[1 $\bar{1}$ 0] and Ni[0 $\bar{1}$ 1]) with an (hkl) plane in Ni parallel to an (HKL) plane in Ag. The (100) and (111) planes of Ni and the (1 $\bar{1}$  $\bar{1}$ ) and (111) planes of Ag are displayed. (b), (c) and (d) superimposed stereograms of Ag (red points) and Ni (blue points) with the coincident Ag(1 $\bar{1}$ 0) and Ni(0 $\bar{1}$ 1) poles circled in green on the edge of the stereograms. Triangle, square and diamond symbols represent poles corresponding to {111}, {100} and {110} planes, respectively. The round symbols in (c) represent the Ni(210) (blue) and Ag(120) (red). In (b) the stereograms are centered on the Ni(111) and Ag(111) planes in a twin OR; in (c) the stereograms are still in twin OR but centered on Ni(100) by rotating both the Ag and Ni stereograms of (b) together by 54.7° about their common <110> axes (circled in green); and in (d) the stereograms are centered on Ni(100) and Ag(1 $\bar{1}$  $\bar{1}$ ) in an oct-cube OR (i.e. a relative rotation of 15.8° of the Ag stereogram in (c) about the common <110> axis). The blue dashed triangles identify the SST of Ni, and the red dashed triangle in (c) is the Ag (1 $\bar{1}$  $\bar{1}$ )-(111)-(120) triangle which contains all Ag poles that result from the observed ORs. In addition, the Ni(111) and Ag(111) poles have been circled in brown in b, c, and d, for easy identification.

In the particular case of the gradual transition of *OR S* observed for Ag on Ni substrates lying along the left edge of the SST, from Ni(100) to Ni(111), an explanation of the OR was provided in our previous study [12], and is summarized here. Consider the sketch in Fig. 2a showing an example of *OR S*, with a Ag film (red) on top of a Ni substrate (blue). Both crystals are viewed along the common <110> directions (Ag[1 $\bar{1}$ 0] and Ni[0 $\bar{1}$ 1]). The range of orientations along the left edge of the SST of Fig. 1 is encompassed by the (100) and (111) facets on the Ni substrate. The corresponding range of planes in the Ag film is shown by the (11 $\bar{1}$ ) and (111) facets facing the Ni facets. For a specific interface, corresponding planes Ag(HKL) and Ni(hkl) are placed in contact. As the Ni surface orientation changes through 54.7° from (111) to (100), the Ag interface orientation changes through 70.5° from (111) to (11 $\bar{1}$ ). The difference of 15.8° describes the range from *OR T* to *OR O* along the left edge of the SST. For a substrate orientation Ni(hkl) lying somewhere between Ni(100) and Ni(111), the angular gap between Ni(hkl) and Ag(HKL) is given by

$$\alpha = \phi - \theta \quad (1)$$

where  $\theta$  is the angle between Ni(hkl) and Ni(111) and  $\phi$  is the angle between Ag(HKL) and Ag(111) planes (all three angles taken to be positive). As shown previously [11,12], both the observed experimental and simulated ORs are well described by a linear model:

$$\phi = (70.5/54.7) \theta \quad (2)$$

The stereograms in Figs. 2b-d illustrate the same range of ORs where several sets of plane normals (i.e. poles) are plotted in a common frame for a pair of crystals. Fig. 2b is a Ag stereogram centered on Ag(111) superimposed on a Ni stereogram, also centered on the (111) pole, in a twin relationship (*OR T*), obtained by a relative rotation of 60° of Ag poles around Ni(111). This also leads to superposition of the Ag[1 $\bar{1}$ 0] and Ni[0 $\bar{1}$ 1] poles circled in green. Fig. 2c plots the same *OR T* with the stereograms centered on Ni(100). This illustrates that the Ag{111} closest to Ni(100) in the twin OR is located 15.8° away. Fig. 2d illustrates *OR O*, centered on Ni(100) and Ag(11 $\bar{1}$ ), showing that the Ag(111) and Ni(111) poles that were superimposed in Fig. 2c are now separated by 15.8°.

To summarize, the Ag ORs along the (100)-(111) edge of the SST vary smoothly from *OR T* on Ni(111) to *OR O* on Ni(100). These ORs can thus be described as a lattice rotation by an angle  $\alpha$  around the common <110> directions. These common directions remain parallel due to the alignment of steps during film growth (and/or equilibration), and the rotation angle  $\alpha$ , which varies from 0° (for *OR T*) to 15.8° (for *OR O*), is given by Eq. 1.

The present paper extends the above approach, restricted to substrate orientations lying along the left edge of the SST from Ni(111) to Ni(100), to predict the special ORs adopted by Ag on all Ni substrate orientations within the (100)-(111)-(210) region of orientation space.

### 3. ANALYSIS of *OR S*

The clear separation between *OR C* and *OR S* is apparent from the green and pink points in the SST shown in Fig. 1. *OR S* denotes a continuous range of ORs from *OR T*, displayed by Ag on Ni orientations that lie along the (111)-(210) line (see Fig. 1), to *OR O*, which occurs on Ni(100). We hypothesize that the same gradual orientation change that occurs for Ni substrates lying along the left edge of the SST, and described in section 2, also occurs along all possible "orientation trajectories" that run from *OR T* at any point along the (111)-(210) line, to *OR O* at Ni(100). Thus, we proceed here to extend that linear model to the remainder of the Ni orientation space where Ag adopts *OR S*. The corresponding Ag and Ni orientation spaces are displayed in Fig. 3. The Ni space on which Ag displays *OR S* is the left blue (100)-(111)-(210) sub-triangle, and the corresponding Ag space is described by the red (111)-(120)-(11 $\bar{1}$ ) triangle, superimposed in a twin relationship (*OR T*) which may be described by a 60° rotation around the common (111) pole.

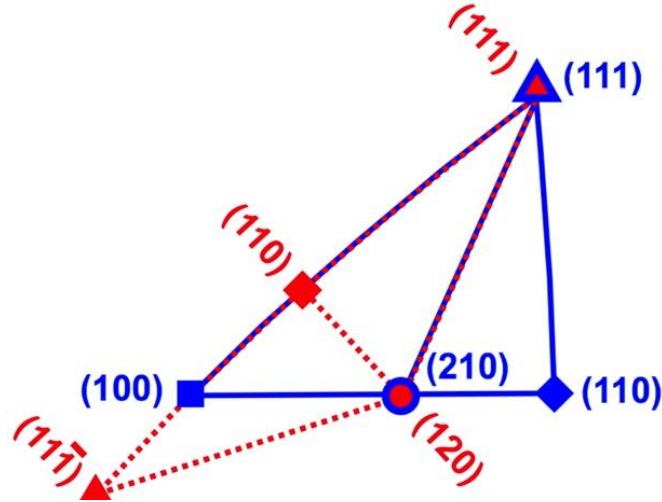


Figure 3. Expanded view of the central portion of Fig. 2c, showing the corresponding orientation space occupied by Ag ((111)-(120)-(11 $\bar{1}$ ), red dotted triangle) on Ni substrate orientations ((100)-(111)-(210), blue triangle)<sup>†</sup>. These twinned stereographic triangles are centered on the Ni(210) and Ag(120) poles and their superimposed right edges, i.e., the Ni (111)-(210) and the Ag (111)-(120) lines, are the traces of the Ni(1 $\bar{2}$ 1) and the Ag(2 $\bar{1}$ 1) planes, respectively.

The process of connecting the Ni(hkl) poles to the Ag(HKL) poles in *OR S* may be visualized as stretching the blue Ni (100)-(111)-(210) triangle into the red Ag (111)-(11 $\bar{1}$ )-(120) twinned triangle. Formally, this process may be written as an axis-angle pair,  $\alpha/\langle 110 \rangle$ , denoting a rotation by an angle  $\alpha$  around a common  $\langle 110 \rangle$  axis. The angle  $\alpha$  is defined relative to *OR T* as a reference. However, *OR T* itself can be obtained from *OR C* by a rotation of 70.5° around  $\langle 110 \rangle$ . Thus, *OR S* may be written as a combined rotation

<sup>†</sup> Since Ag interface plane orientations can range from (111) to (11 $\bar{1}$ ), they naturally stretch over two stereographic triangles. Of course, planes in the second stereographic triangle may always be remapped into a single triangle by means of a suitable cubic symmetry operation, but this would obscure the simple relationship illustrated in Fig. 3.

$\beta/\langle 110 \rangle$  (with  $\beta = 70.5^\circ - \alpha$ ), describing the fixed twinning operation, followed by the variable rotation  $\alpha$ . This rotation  $\beta/\langle 110 \rangle$  can be written explicitly as  $R(\beta)^\ddagger$  so that

$$(HKL) = R(\beta) (hkl) \quad (3)$$

where

$$R(\beta) = \begin{pmatrix} \frac{\sin \beta}{\sqrt{2}} & -\frac{1}{2}(1 - \cos \beta) & \frac{1}{2}(1 + \cos \beta) \\ \frac{\sin \beta}{\sqrt{2}} & \frac{1}{2}(1 + \cos \beta) & -\frac{1}{2}(1 - \cos \beta) \\ -\cos \beta & \frac{\sin \beta}{\sqrt{2}} & \frac{\sin \beta}{\sqrt{2}} \end{pmatrix}$$

To obtain the angle  $\beta = 70.5^\circ - \alpha$  for a given (hkl), we use the fact that  $\alpha = 0^\circ$  along the Ni (111)-(210) line of the Ni SST, where Ag adopts *OR T*. With increasing distance from this line,  $\alpha$  increases up to  $15.8^\circ$  at Ni(100), where Ag adopts *OR O*. Assuming this dependence to be linear, we can obtain  $\alpha$  for any Ni(hkl) as follows. Since the Ni (111)-(210) line is the trace of the Ni( $\bar{1}\bar{2}1$ ) plane, the angular distance between Ni(hkl) and the Ni( $\bar{1}\bar{2}1$ ) trace is  $\varepsilon$ , where  $(90^\circ - \varepsilon)$  is the angle between (hkl) and the ( $\bar{1}\bar{2}1$ ) plane normal. As Ni(hkl) changes from a position anywhere along the trace of the Ni( $\bar{1}\bar{2}1$ ) plane to Ni(100), the angle  $\varepsilon$  changes from 0 to  $24.1^\circ$ , while the angle  $\alpha$  changes from 0 to  $15.8^\circ$ . For the linear model, this relationship is

$$\alpha/15.8^\circ = \varepsilon/24.1^\circ \quad (4)$$

Using the small angle approximation,  $\varepsilon/24.1^\circ \approx \sin \varepsilon / \sin 24.1^\circ = \cos(90^\circ - \varepsilon) / \cos(90^\circ - 24.1^\circ) = (hkl) \cdot (\bar{1}\bar{2}1) / (100) \cdot (\bar{1}\bar{2}1) = (hkl) \cdot (\bar{1}\bar{2}1) / (1/\sqrt{6}) = (h-2k+l) / \sqrt{(h^2 + k^2 + l^2)}$ . With this approximation,  $\alpha$  can be written directly as a function of hkl using Eq. 4:

$$\alpha = 15.8^\circ (h - 2k + l) / \sqrt{(h^2 + k^2 + l^2)} \quad (5)$$

An example of the use of the above procedure to obtain the computed orientation of the Ag interfacial plane, Ag(HKL), for the case of *OR S*, is given in Appendix A. The experimental value of Ag(HKL) may be obtained directly from the experimental EBSD data [11] as the  $a_{13}$ ,  $a_{23}$  and  $a_{33}$  coefficients of the orientation matrix [22]. The mean absolute deviation between the calculated and measured values of Ag(HKL) obtained from over 90 measurements averages  $2.3^\circ$ . This is rather good agreement, given that the experimental error in measuring the Ni(hkl) can be as large as about  $3^\circ$ .

---

<sup>‡</sup>  $R(\beta)$  was obtained from the standard expression for a rotation  $\beta$  around a  $[0\bar{1}1]$  direction, followed by a cubic symmetry operation (a fourfold rotation) in order to match the specific indices to those chosen in the figures.

## 4. DISCUSSION

The linear model of the previous section is independent of any physical or chemical attributes of Ni and Ag. At first glance, this appears to indicate that strains or defects due to lattice mismatch are unimportant, and that the phenomenon is controlled entirely by geometric or crystallographic parameters. This conclusion is surprising because lattice mismatch is known to play a key role in the structure and properties of interfaces, and the mismatch between the Ag and Ni lattices is about 16%, which is significant.

To solve this apparent paradox, we explore the possible role of lattice mismatch for the interface in some detail. First, we investigate the effect of size misfit at steps in a 1-dimensional (1D) approach, followed by a more complete 2D approach. It will be shown that these models provide additional physical insight into the origin of the systematically variable *OR S* while remaining fully consistent with the experimentally observed data.

### 4.1. The role of steps and lattice mismatch in *OR S*

As indicated above, our previous work [11] has noted that the steps on both sides of the Ni/Ag interfaces are parallel to each other and that this is consistent with the observation that the Ni[0 $\bar{1}$ 1] and Ag[1 $\bar{1}$ 0] directions that lie closest to the interfacial planes in both the Ni substrate and the Ag film are aligned (to within  $0.9^\circ \pm 0.8^\circ$ ). This suggests that film growth occurs by atomic attachment at step edges, leading to a natural alignment of terraces and steps. However, the difference in lattice parameters between the substrate and the film implies that at any step, there is a mismatch in the spacing of terrace planes, which can lead to a macroscopic rotation of the lattices around the step direction [21,23].

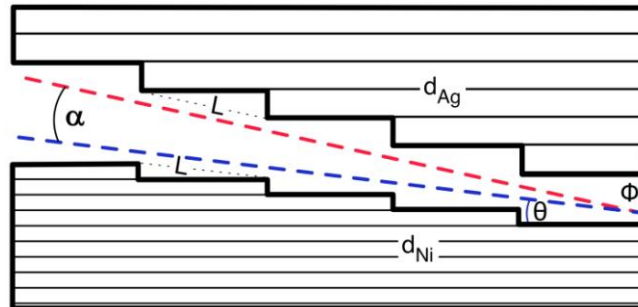


**Figure 4.** Schematic illustration of the lattice rotation caused by the difference in step height at a vicinal interface, showing the relationship between terraces, steps and angles of inclination ( $\theta$  and  $\phi$ ) and rotation  $\alpha$ .

The macroscopic lattice rotation is related to the mismatch and the step density. This allows the prediction of the Ag interface orientation (HKL) for any Ni surface orientation (hkl), where Ag(HKL) and Ni(hkl) are described by their angles  $\phi$  and  $\theta$  to the (111) planes in Ag or Ni, respectively, as defined earlier (see Fig. 2a). Consider Fig. 4; if the distance between step edges is  $L$  and the step height is  $d$ , then the angle of the

stepped interface plane to the nearby terrace plane is  $\sin \phi = d_{\text{Ag}}/L$  in Ag and  $\sin \theta = d_{\text{Ni}}/L$  in Ni. This yields the following relationships between  $\phi$  and  $\theta$ :

$$\sin \phi = (d_{\text{Ag}} / d_{\text{Ni}}) \sin \theta \quad (6)$$

and the rotation  $\alpha$  is obtained from Eq. 1. As written here in Eq. 6, and described in Fig. 4, the interfacial geometry has been simplified for the case where the terraces on both sides of the interface are taken to be (111) planes. The general case is somewhat more complex, as described in more detail below in section 4.2.1.3. Thus, if the width  $L$  is identical in the two crystals<sup>§</sup>, the difference in step height  $d$  leads to different inclinations  $\phi$  and  $\theta$ , with an angular gap of  $\alpha$ . Bringing the two crystals into contact along the interface requires a rotation  $\alpha$  to close the angular gap. This rotation ensures that the terrace planes meet edge-to-edge in the interface [23].

The relationship of this geometrical description to moiré patterns and the reciprocal space  $\Delta\mathbf{g}$  description is summarized in Appendix B.

## **4.2. Advantages of the twin over the cube-on-cube OR**

From the simple argument presented in Fig. 4, one might expect a lattice rotation  $\alpha$  for all vicinal surfaces in heteroepitaxial systems where the step height depends on the lattice parameters. However, this effect is observed for *OR S* only, but not for *OR C*. To understand this critical difference it is necessary to consider the mismatch of the other lattice planes *across* the interface. This requires an extension to a 2D description of the 1D model based on edge-to-edge matching of a single set of planes (the terraces).

### **4.2.1. The role of lattice mismatch in 2D edge-to-edge matching across the interface**

#### **4.2.1.1. 2D view of edge-to-edge matching in the direct space**

To see this effect in 2D, consider the mismatch of corresponding lattice planes across a vicinal interface for *OR C* and *OR S*. For *OR C*, all corresponding planes in Ni and Ag have the same Miller indices (i.e.,  $(hkl)=(HKL)$ ) and are parallel, even though the lattice constant of Ag is 16% larger than that of Ni. For *OR S*, corresponding planes generally have different Miller indices (i.e.,  $(hkl)\neq(HKL)$ ) with varying mismatch. For a Ni substrate vicinal to (111), and rotated by  $\theta=12^\circ$  towards (100), the Ag lattice must be rotated by an angle  $\alpha=2^\circ$  to allow the (111) terrace planes of Ag and Ni to meet edge-to-edge along the interface, as suggested by the 1D model (Fig. 4). Figure 5 illustrates two possible 2D views of the near-interface region. Figure 5a is an *OR C* representation of the interface, where the near-horizontal  $\{111\}$  terrace planes meet edge to edge, but the mismatch of the planes inclined to the interface is apparent. In contrast, Fig. 5b illustrates the structure expected for *OR S*, where the stacking of  $\{111\}$  terrace planes across the interface is reversed in

---

<sup>§</sup> Due to the discrete nature of a crystal,  $\alpha$ ,  $\theta$ ,  $\phi$  and  $L$  are not strictly continuous variables.

twin-like fashion. Here the small rotation of  $\alpha=2^\circ$  that allows terrace planes to meet edge-to-edge also improves the match of other planes across the interface, as is evident from Fig. 5b.

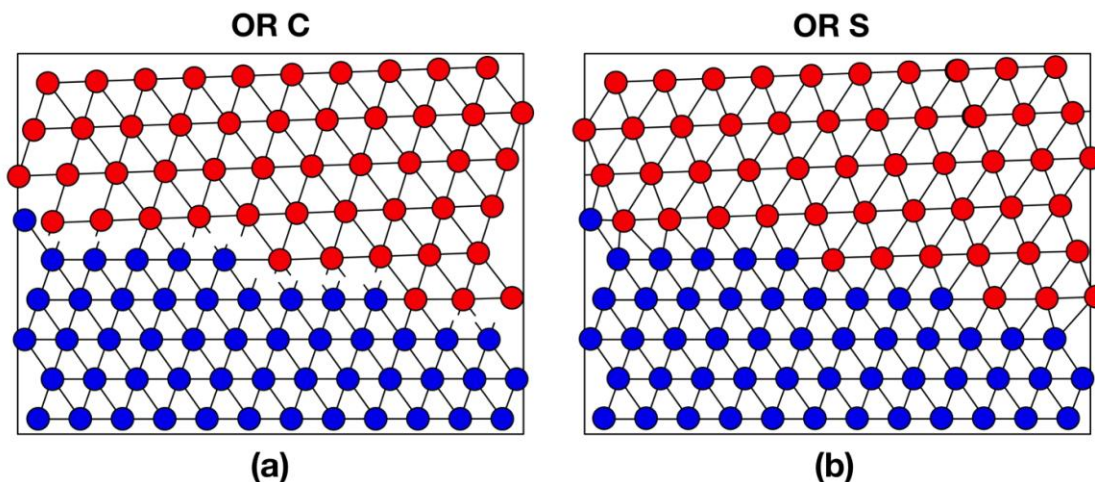


**Figure 5.** Vicinal interface with a small lattice rotation  $\alpha$  to allow terrace planes to meet edge-to-edge in the interface. (a) Schematic of *OR C* showing “broken bonds” between corresponding planes that arise because of the 16% lattice mismatch. (b) Schematic of *OR S* showing continuity of all corresponding planes meeting edge-to-edge in the interface. This interface makes an angle of  $\theta=12^\circ$  with the horizontal Ni(111) plane (i.e. from (111) towards (100)), corresponding to a rotation of  $\alpha=2^\circ$  of the Ag lattice.

Although Fig. 5 illustrates the principal features that distinguish the behavior of vicinal interfaces in *OR C* and *OR S*, the subtleties of lattice matching at the interface are not easy to see because structural changes due to small rotations can only be seen over long segments of the interface. These effects are particularly difficult to visualize as the substrate orientation changes. This is where moiré patterns and a reciprocal space representation in terms of  $\Delta\mathbf{g}$  vectors are more useful as illustrated in Appendix B [5,6,24-26].

#### **4.2.1.2. $\Delta\mathbf{g}$ representation of edge-to-edge matching in reciprocal space**

Appendix B shows that the difference vector  $\Delta\mathbf{g}$  between two reciprocal lattice vectors defines the unique interface (perpendicular to this  $\Delta\mathbf{g}$  vector) where the two corresponding lattice planes meet edge-to-edge. This is a 1D matching criterion. To compare the behavior of  $\Delta\mathbf{g}$  vectors for different ORs in 2D, Fig. 6 shows superimposed diffraction patterns of Ni (blue) and Ag (red) seen along the common  $\langle 110 \rangle$  close-packed direction. The central Fig. 6b illustrates the reciprocal lattice for *OR T* while the figures to the left and right show the effect of rotations by  $\pm 15.8^\circ$  of the Ag pattern, respectively. This choice of rotation angles was made because  $+15.8^\circ$  is the value of  $\alpha$  which leads to *OR O*, whereas the same rotation in the opposite direction is never observed. For the sake of clarity, the Ni substrate lattice is held fixed, with the Ni(111)  $\mathbf{g}$ -vector pointing north to correspond to the substrate lattice in Figs. 4 and 5.

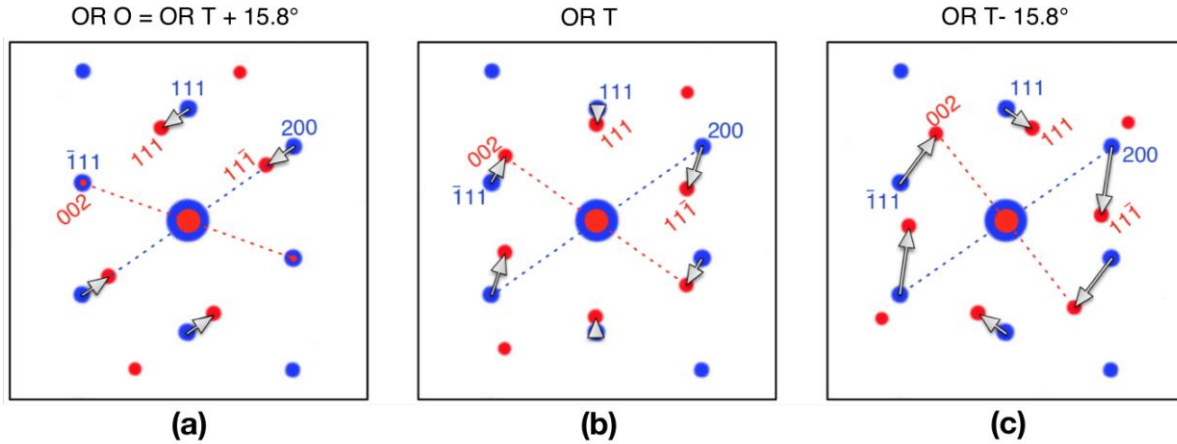


**Figure 6.** Reciprocal space representation of superimposed  $\langle 110 \rangle$  diffraction patterns illustrating the asymmetric effects of a  $\pm 15.8^\circ$  rotation from  $OR T$  (b). Ni  $[0\bar{1}1]$  shown in blue and Ag  $[\bar{1}\bar{1}0]$  in red. A  $+15.8^\circ$  rotation (counter clockwise) of the Ag pattern in (a) leads to  $OR O$ , while the equivalent rotation in the opposite sense, a  $-15.8^\circ$  rotation (clockwise) in (c), leads to an OR which is never observed. Arrows show  $\Delta\mathbf{g}$  vectors for corresponding lattice planes in the two crystals. Dotted lines mark (200)  $\mathbf{g}$ -vectors in both phases.

Between Figs. 6a and 6b the orientation relationship changes from  $OR O$  to  $OR T$ , covering the same range as shown in Fig. 2. Notice the behavior of the  $\Delta\mathbf{g}$  vectors, represented by arrows connecting corresponding diffraction spots. In Figs. 6a and 6b, all  $\Delta\mathbf{g}$  vectors are (nearly) parallel to each other, indicating that all the lattice planes crossing an interface that lies normal to  $\Delta\mathbf{g}$  meet (nearly) edge-to-edge, leading to low energy interfaces with good matching at the atomic scale. In contrast, the orientation relationship in Fig. 6c shows diverging  $\Delta\mathbf{g}$  vectors, implying large mismatch for planes inclined to the interface, i.e., planes whose difference vector  $\Delta\mathbf{g}$  is inclined to the interface normal. This explains why the OR of Fig. 6c, at  $OR T - 15.8^\circ$ , is never observed, and why, starting from  $OR T$ , the lattices show a continuous range of rotations in one sense (toward  $OR O$ ), but no rotations at all in the opposite sense, where instead,  $OR C$  is preferred. This asymmetric behavior of lattice rotations  $\alpha$  is associated with an asymmetric range of Ni(hkl) surfaces. As the surface orientation changes from Ni(111) to Ni(100),  $\alpha$  changes from 0 to  $15.8^\circ$ . But if the surface orientation changes in the opposite direction, from Ni(111) toward Ni( $11\bar{1}$ ), any rotation  $\alpha$  would only increase the mismatch, thus leading to a preference for  $OR C$ . In the SST, this different behavior in opposite directions can be seen along different edges: along the Ni (111)-(100) edge, the Ag OR rotates from  $OR T$  to  $OR O$ , while along the Ni (111)-(110) edge, Ag maintains  $OR C$ . As shown in the next section, this implies a significant difference in the role of steps that describe vicinal surfaces in the terrace-ledge-kink (TLK) model commonly used in surface science.

#### **4.2.1.3. Asymmetry of $\langle 110 \rangle$ edges in the TLK model**

The asymmetry of rotations can also be seen in the crystallography of ledges on both sides of the Ni/Ag interface. Using the terrace-ledge-kink (TLK) model of surfaces [27], it is possible to decompose any

surface orientation (hkl) into terraces and steps, and to further decompose any steps into ledges and kinks. According to van Hove and Somorjai [28], any (hkl) surface may be decomposed into three linearly independent microfacet orientations, with the microfacet of largest area being identified as the terrace, the one with intermediate area as the ledge, and the one with smallest area as the kink. We choose the (100), (111) and (11 $\bar{1}$ ) planes as the three basic microfacet orientations.

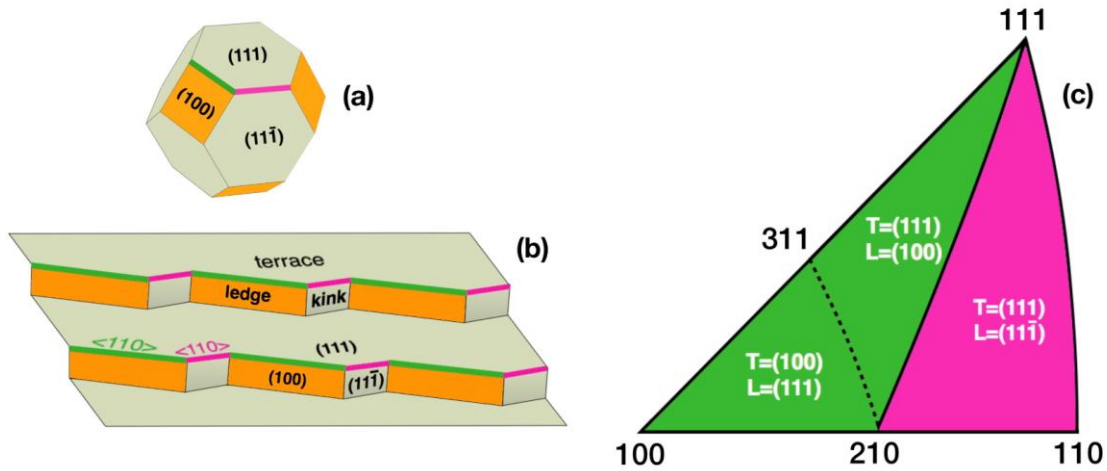


**Figure 7.** (a) Cuboctahedral shape of a Ni crystal with orange (100) and beige (111) facets on which two different kinds of  $\langle 110 \rangle$  edges are marked in green (between (100) and (111) facets) and pink (between two {111} facets); (b) sketch of a Ni surface with (111) terraces, (100) ledges and (11 $\bar{1}$ ) kinks, according to the TLK model, with the color code for facets and edges used in (a); (c) Ni SST showing combination of terraces T and ledges L in different domains. Ni surfaces in the left half of the SST, marked in green, have  $\langle 110 \rangle$  edges connecting terraces and ledges of mixed type. Ni surfaces in the right half of the SST, marked in pink, have  $\langle 110 \rangle$  edges connecting terraces and ledges of the same {111}-type microfacets.

Fig. 7a shows a cuboctahedral crystal shape (calculated using Wulffmaker [29]) which illustrates that, for this choice of facets, there can only be two kinds of junctions between microfacets depending on whether they connect two {111}s or a {111} to a {100} facet, but all of these junctions must run along  $\langle 110 \rangle$  type directions. In Fig. 7a, the two types of junctions are marked in pink and green, respectively.

Fig. 7b is an example of a Ni surface in the top left of the SST, decomposed into (111) terraces, (100) ledges and (11 $\bar{1}$ ) kinks. The colors of facets and  $\langle 110 \rangle$  edges match those used in Fig. 7a.

Fig. 7c shows the SST, divided into three regions, characterized by the microfacet planes of the terrace (T) and the ledge (L), as dictated by the TLK model. Along the left and right edges of the SST, kinks are absent, and surfaces are made up entirely of terraces and ledges. On the left, and starting from the (111) plane, the step density initially increases with increasing angle ( $\theta$ ) of the macroscopic substrate surface from the Ni(111) terrace plane. At the mid point, in the vicinity of the Ni(311) orientation, i.e., where the (12 $\bar{1}$ ) trace shown as a dashed line intersects the (111)-(100) left edge, the T=(111) terraces and L=(100) ledges exchange roles. Below this point, T=(100) and L=(111), and the step density then decreases as Ni(100) is

approached. Regardless of their exchanging roles, terraces and ledges along the left edge are always of mixed type, with one being (111) and the other (100). Along the right edge of the SST, kinks on the Ni substrate are also absent. Terraces and ledges have (111) and (11 $\bar{1}$ ) orientations, respectively. The step density increases as the angle increases away from (111) towards (110), where the area of terraces and ledges becomes identical.

When the Ni(hkl) surface lies within the SST, i.e. away from its left and right edges, the steps are made up of ledges and kinks. Along the (100)-(210) central dividing line, ledges and kinks have the same area, and their areas relative to the (111) terrace increase with angle away from Ni(111), until all three microfacets eventually become equal at Ni(210). This central line separates two halves of the SST, which are colored according to the two types of  $\langle 110 \rangle$  edges between their terrace and ledge orientations, as in Fig. 7a. These two domains also describe the regions of existence of *OR S* and *OR C*, shown previously in Fig. 1.

To understand the observed ORs in the framework of this TLK model, consider the lattice rotations described in Figure 6. The lattice rotation from Fig. 6b to 6a corresponds to the change from *OR T* to *OR O*, which allows edge-to-edge matching of all or most lattice planes crossing the interface ( $\Delta\mathbf{g}$  vectors aligned). This describes the behavior at steps between mixed facets (i.e. green  $\langle 110 \rangle$  edges), which leads to a Ag lattice relative rotation of between 0 and 15.8° around the  $\langle 110 \rangle$  common direction. By comparison, a lattice rotation in the opposite sense (Fig. 6c), would lead to increased mismatch between most Ag and Ni planes crossing the interface (diverging  $\Delta\mathbf{g}$  vectors), and is therefore unfavorable. This describes the behavior at steps between  $\{111\}$  facets, as found in the pink region along the right edge of the SST.

Along the entire line separating the green and pink halves of the SST, *OR T* is maintained and hence no lattice rotation is observed. This may seem surprising since along this line, going from (111) to (210), the relative area of (100) microfacets connected by a green  $\langle 110 \rangle$  edge increases. However, the area of (11 $\bar{1}$ ) microfacets connected by a pink  $\langle 110 \rangle$  edge increases in equal proportion, and it can be argued that any gain from a lattice rotation around the green edge would be offset by the cost of accommodating this rotation along the microfacet connected by a pink  $\langle 110 \rangle$  edge. In the left half of the SST, the (11 $\bar{1}$ ) microfacet is the smallest of the three, and hence serves as the kink. The same balance holds for any lines in the green section of the SST that are parallel to the central dividing line. Along all such parallels, going from the left edge to the bottom edge of the SST, ledge and kink facet junctions are added to the Ni substrate surface in equal proportion and thus cause no lattice rotation beyond that which is determined by the relative fraction of mixed terraces and ledges along the left edge of the SST (Eq. 6). The fact that these parallels are defined by their distance from the trace of the (1 $\bar{2}$ 1) has been used to determine the lattice rotation  $\alpha$  in Eqs. 4 and 5.

Recall that the Ag interface plane, whether in *OR S* or *OR C*, always lies in the (111)-(210)-(110) triangle, so that the Ag terrace and ledge are always both of  $\{111\}$  type (except along the (111)-(210) line where ledges and kinks are of equal size). Thus, the terrace/ledge surface orientations in Ni and Ag will be different in the *OR S* region, whereas they will be identical in the *OR C* region. This difference emphasizes the

key role of terrace-ledge junctions of Ni on the OR:  $\{111\}$ - $\{100\}$  edges (green) lead to a relative lattice rotation  $\alpha$  about  $\langle 110 \rangle$  to optimize the edge-to-edge matching in 2D, while kinks just lock out any further lattice rotation in either of the ORs.

#### **4.2.2. Twin correspondence and 2D transformation matrix**

In this section, we employ the phase transformations approach to minimize the interfacial mismatch for heteroepitaxial films using the strain ellipse, e.g. [9,30,31], which provides a graphical representation of the transformation strain for a given lattice correspondence.

Lattice correspondence relationships are essential to our understanding of phase transformations, e.g. [8,32]. For cubic crystals, the most common is the cube correspondence, used as a reference to describe the misorientation between grains across grain boundaries, and the Bain correspondence, used to describe the relation between FCC austenite and BCT martensite, or more generally, between FCC and BCC crystals. Any lattice correspondence implies a homogeneous strain to accomplish the phase transformation. For the cube correspondence, the transformation from one crystal into the one adjacent at the grain boundary is simply a rotation about a common axis. For the Bain correspondence this is an expansion along a common cube axis and a contraction along orthogonal directions. Numerous ORs in cubic heterophase systems are based on the Bain correspondence. By comparison, the twin correspondence, although well established in the context of deformation in single-phase systems, has received much less attention as a lattice correspondence in heterophase systems. For the twin correspondence, the homogeneous deformation is a simple shear parallel to the twin plane (the twinning shear).

The twin correspondence for Ag-Ni is apparent from Fig. 6, where  $\Delta\mathbf{g}$  vectors have been drawn to connect *corresponding*  $\mathbf{g}$ -vectors. One may think of the  $\Delta\mathbf{g}$  vectors as a graphical shorthand notation for " $\mathbf{g}_1$  corresponds to  $\mathbf{g}_2$ ". Once two sets of corresponding planes have been chosen, the lattice correspondence is fully determined (the fact that the common  $\langle 110 \rangle$  directions define the axis of rotation and remain parallel throughout reduces the correspondence to 2-dimensions)\*\*. Fig. 6b illustrates why this is referred to as the twin correspondence (the vertical  $\{111\}$  planes in Ag and Ni are aligned, while the  $\{200\}$  planes in Ag and Ni appear mirrored to the right and left of the vertical, respectively). It can be seen by inspection that the transformation of the blue Ni pattern to the red Ag pattern can be described as a simple shear in the vertical direction combined with a uniform contraction  $1/\rho$  (corresponding to a uniform expansion  $\rho$  in real space where  $\rho$  is the lattice parameter ratio,  $a_{\text{Ag}}/a_{\text{Ni}}=1.16$ ). Although the  $\Delta\mathbf{g}$  vectors change with rotation, the lattice correspondence is the same for all three panels of Fig. 6 (i.e. the same pairs of  $\mathbf{g}$ -vectors are connected). For this correspondence,  $\mathbf{g}_{111}$  in Ni corresponds to  $\mathbf{g}_{111}$  in Ag and  $\mathbf{g}_{200}$  in Ni corresponds to  $\mathbf{g}_{11\bar{1}}$  in Ag. It is then

---

\*\* Note that in 3D, this correspondence involves an additional shear component along the  $[\bar{1}10]$  axis of projection. This can be seen by considering that the same twin can be generated by a shear in three equivalent  $\langle 211 \rangle$  directions. Only one of these lies in the plane of projection, while the other two are inclined at  $60^\circ$  and hence project as only half the true shear.

possible to write the homogeneous deformation that takes the Ni lattice to the corresponding Ag lattice as the transformation matrix:

$$A = \rho \begin{pmatrix} 1 & s \\ 0 & 1 \end{pmatrix} \quad (7)$$

where  $s=0.35$  is the magnitude of the simple shear. This transformation is directly visible from the  $\Delta\mathbf{g}$  vectors in Fig. 6b. The red pattern is contracted by a factor  $\rho$  relative to the blue pattern. Reversing this contraction would bring the vertical red and blue  $\mathbf{g}_{111}$  vectors into coincidence while aligning the other  $\Delta\mathbf{g}$  vectors along the vertical direction – thereby providing a visual representation of a simple shear of magnitude 0.35 (see for example [31]).

In matrix form, the lattice rotation  $R'$  can be included in the transformation as follows:

$$R' A = \begin{pmatrix} \cos \alpha & \sin \alpha \\ -\sin \alpha & \cos \alpha \end{pmatrix} \rho \begin{pmatrix} 1 & s \\ 0 & 1 \end{pmatrix} \quad (8)$$

Solving this equation for its eigenvalues  $\lambda_{1,2}$  and eigenvectors  $v_{1,2}$  gives the relationship between  $\alpha$  and the interface plane (containing the eigenvector with the smaller of the two eigenvalues, i.e. the smaller strain):

$$\lambda_{1,2} = \rho/2 (B \pm \sqrt{B^2 - 4}) \quad (9)$$

$$v_{1,2} = \left\{ \frac{1}{2} \left( -s \mp \frac{\sqrt{B^2 - 4}}{\sin \alpha} \right), 1 \right\} \quad (10)$$

To simplify these equations, we have defined  $B$  as  $B=(2 \cos \alpha - s \sin \alpha)$ . Notice that for  $s=-0.35$ ,  $\alpha$  can only take values between  $0^\circ$  and  $20^\circ$ . Outside of this range of ORs, the term in the square root is negative, and there are no real solutions for the eigensystem. Note that at the extreme ends of the OR, where  $B^2=4$  and  $\alpha=0^\circ$  or  $\alpha=20^\circ$ , the two eigenvectors  $v_{1,2}$  as well as the two eigenvalues  $\lambda_{1,2}$  become identical. This degeneracy signals the limit of favorable rotations because any lattice rotation beyond these values leads to the disappearance of all eigenvectors. In other words, outside this range of rotations, there are no directions that are unrotated during the transformation.

A graphical representation of this transformation in the form of the strain ellipse (e.g. [31]) is shown in Fig. 8. The transformation deforms the blue circle (representing Ni) into a red ellipse (representing Ag). The large ellipse represents the transformation in real space and the small ellipse orthogonal to it represents the transformation in reciprocal space. The transformation strains (short vectors connecting corresponding points on the circle and the ellipses) are shown as hollow arrows (real space) and solid arrows (reciprocal space,  $\Delta\mathbf{g}$  vectors in diffraction patterns). Eigenvectors (unrotated directions) are visible as radius vectors of the circle that do not change their direction during the transformation to the ellipse. Eigenvectors are easily recognized in this schematic because their strain vectors point in a radial direction. In Fig. 8, eigenvectors are shown as

large radius vectors extended or contracted from their position on the blue circle (Ni) to the corresponding position on a red ellipse (Ag).

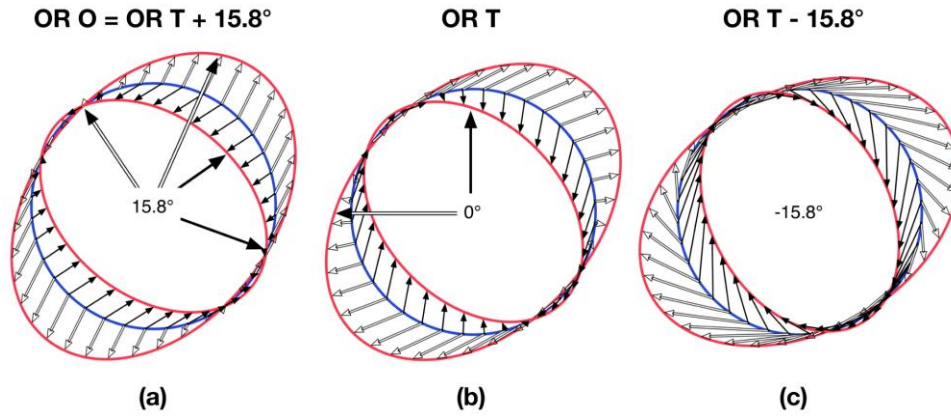


**Figure 8.** Strain ellipse showing the effect of lattice rotation in real and reciprocal space, corresponding to the  $\Delta\mathbf{g}$  representation in Fig. 6. Blue circle represents Ni. Red ellipses represent Ag - large ellipse for real space, small orthogonal ellipse for reciprocal space. Small open (or solid) arrows indicate the strain (or  $\Delta\mathbf{g}$ ) vectors describing the transformation in real (or reciprocal) space, respectively. Eigenvectors, shown here as large radius vectors, remain unrotated in the transformation and are thus readily recognized by the fact that they are aligned with their strain (or  $\Delta\mathbf{g}$ ) vectors. Eigenvectors in real and reciprocal space are denoted by hollow and solid arrows, respectively, and are pairwise normal to each other. In a) it can be seen that the eigenvector with the larger strain in one space is normal to the eigenvector with the smaller strain in the other space (e.g. [30]). Starting from  $OR\ T$  in b), a  $15.8^\circ$  rotation leads to  $OR\ O$  in a) whereas a  $-15.8^\circ$  rotation (shown in c) is never observed. Notice the alignment of strain (or  $\Delta\mathbf{g}$ ) vectors in a) and their dispersion in c). Also note the absence of eigenvectors in c). In b) the eigenvectors in each space are degenerate, i.e. identical in direction and magnitude, while they remain orthogonal between real and reciprocal space.

Figure 8 illustrates how the addition of a lattice rotation  $\alpha$  affects the length and orientation of the strain vectors and the eigenvectors [33]. The ORs in Figs. 8a-c are identical to those presented in Figs. 6a-c. The strain ellipse shown in the center (Fig. 8b) depicts the transformation in  $OR\ T$ . A rotation of the Ag ellipses by  $15.8^\circ$  relative to the stationary Ni circle results in  $OR\ O$  (Fig. 8a). Here the eigenvectors enclose an angle of  $\sim 60^\circ$  each in real space (hollow) and reciprocal space (solid). It can be seen that eigenvectors in real space are pairwise orthogonal to eigenvectors in reciprocal space [31].

Note that  $OR\ O$  is special because at  $\alpha=15.8^\circ$  a direction in the Ni(100)/Ag(11 $\bar{1}$ ) interface is strain-free (an eigenvector with  $\Delta\mathbf{g}=0$ , i.e. the small hollow arrow vanishes)<sup>††</sup>. It can be seen that all strain (or  $\Delta\mathbf{g}$ ) vectors are aligned in  $OR\ O$  and nearly aligned in  $OR\ T$ . By comparison, they diverge for the hypothetical OR at  $\alpha=-15.8^\circ$  shown in Fig. 8c.

As the OR changes from Fig. 8a to b, eigenvectors move closer to each other in both, real and reciprocal space until they coincide (i.e. become degenerate) at the critical value of  $\alpha=0^\circ$  in Fig. 8b. Any

<sup>††</sup> To be exactly strain-free (an invariant line), the corresponding eigenvalue  $\lambda_i$  must equal unity, which requires  $\alpha=15.1^\circ$  (see Eq. 9). An explicit solution for the case of an invariant line has been given by Xiao and Howe [30] (their Eq. 8).

further rotation eliminates all eigenvectors, as shown for an arbitrarily chosen rotation of  $-15.8^\circ$  in Fig. 8c. An animated graphic to illustrate the behavior of eigenvectors during lattice rotation is provided in the supplementary materials.

In phase transformations, the question typically asked is which interface direction (and associated lattice rotation  $\alpha$ ) has the lowest energy [1,4,8]. A precipitate will tend to maximize its dimension along this direction [31]. This criterion generally predicts an invariant line strain with a unique interface and lattice orientation. However, in the current problem of thin film growth, the substrate orientation (hkl) is fixed, and the question becomes which lattice rotation  $\alpha$  has the lowest energy for a fixed substrate orientation (hkl).

We postulate that for a given substrate orientation (hkl) along the left edge of the SST, the interface must contain an eigenvector of the transformation because any strain with a component normal to the interface would accumulate long-range elastic stresses or require dislocation arrays to accommodate the strain. Naturally, the interface with the smaller of the two eigenstrains is preferable. It can be shown that the interface containing the smaller of the two eigenstrains is normal to the larger of the two eigenstrains in reciprocal space (i.e., the larger  $\Delta\mathbf{g}$  vector also visible in Fig. 8).

The eigenvector in the interfaces is the 2D equivalent of the 1D criterion of edge-to-edge matching. The two criteria predict very similar ORs, but only the 2D analysis can explain why no lattice rotations are observed for *OR C*, even if the terrace planes in the two phases have different spacings. Consider the transformation matrix describing *OR C*, which is a pure expansion of magnitude  $\rho=1.16$ . For a pure expansion, the strain ellipse becomes a circle, and all displacements are radial. Hence every vector is an eigenvector, and any rotation  $\alpha$  will rotate all the strain vectors (or  $\Delta\mathbf{g}$  vectors), thus eliminating all eigenvectors (which by definition are unrotated), similar to the case shown in Fig. 8c. This implies that for any interface, the 2D strain will have components normal to the interface, even if one set of planes meets edge-to-edge (see Fig. 5a). This would lead to prohibitive long-range stresses. Thus, the orientation relationship for *OR C* is effectively locked by the fact that any lattice rotation eliminates all eigenvectors. This is clearly different for the twin correspondence, where a suitable lattice rotation can be chosen to align the smaller eigenvector with the substrate surface, using Eq. 10, which also determines the appropriate rotation  $\alpha$ .

It is interesting to note that the directions of the eigenvectors (Eq. 10) are independent of the lattice parameter ratio  $\rho$  whereas the eigenvalues (Eq. 9) are directly proportional to  $\rho$  (see also animated graphics V1 and V2 in supplementary materials). This implies that the limiting rotation that brings eigenvectors into coincidence does not depend on the lattice parameters, and hence the range of allowable orientations is independent of the combination of materials, for a given lattice correspondence. The range of rotations from *OR T* to *OR O* is given by the twin lattice correspondence alone and is thus valid for all heteroepitaxial systems, independent of lattice parameter ratio. This explains why the same ORs are found in a number of heteroepitaxial systems [34]. However, the eigenvalues depend directly on the lattice parameters, and since only small strains (eigenvalues close to  $\lambda=1$ ) can be accommodated in the interface, it is not unreasonable that only a limited range of systems exhibits *OR O*. This also offers an interesting solution to the apparent

paradox between the conclusions of the linear approximation (rotation independent of  $\rho$ ) and 2D model (rotation dependent on  $\rho$ ).

#### **4.3 Quantitative comparison of different models and experimental data**

In addition to the three models presented above – the linear, the 1D and the 2D model - this interface can also be described by the topological model of Pond et al. [35], which assumes that the terraces are strained to be coherent and the steps are spaced to compensate for the coherency strain. In this model a geometrically invariant interface is relaxed into coherent patches separated by disconnections, which have both step and dislocation character. The relaxed interface contains alternating regions of compression and expansion, which cancel each other at a small distance from the interface. A comparison between the phenomenological theory of martensitic transformations (PTMC) [36] and the topological model initially indicated that the predicted ORs were essentially identical, but the habit planes were significantly different [35]. However, this difference in habit planes was almost entirely due to a sign error, and when corrected, the predictions of the topological model agreed with those of the PTMC [8]. For the case of Ag on Ni, the large 16% strain in the terrace plane is unlikely to be accommodated elastically, but the formalism of the topological model remains valid.

In this model the rotation angle  $\alpha$  is mainly due to the difference in step height, which determines the z-component of the Burgers vector associated with a disconnection. This is also the concept underlying the edge-to-edge matching, and it is not therefore surprising to find that the different approaches predict essentially the same ORs, even for the present case, where the interface is not generally an invariant plane.

For a more quantitative comparison of the different models, we use a plot of the angle  $\theta$  between the interface and the Ni(111) plane versus the rotation angle  $\alpha$ . Each of the models assumes that interfaces in the *OR S* regime are described by these two angles. It is the relationship between  $\theta$  and  $\alpha$  that distinguishes the models from each other. We can therefore use a plot of  $\theta$  versus  $\alpha$  to compare the models with each other and with the experimental data.

The linear model assumes that  $\phi = (70.5/54.7) \theta$  (Eq. 2), and since  $\alpha = \phi - \theta$  (Eq. 1), we can write  $\theta(\alpha)$  as:

$$\theta = (54.7/15.8) \alpha \quad (11)$$

The edge-to-edge matching in the 1D model requires that  $\sin \phi = 1.16 \sin \theta$  (Eq. 6). Using  $\alpha = \phi - \theta$ , we find:

$$\theta = \arctan(\sin \alpha / (1.16 - \cos \alpha)) \quad (12)$$

The topological model (Eq B.8 in [35]<sup>\*</sup>) proposes that:

$$\alpha = (b_z/h) \tan \theta \quad (13)$$

where  $b_z$  is the difference in step heights and  $h$  is the smaller of the two step heights.

Finally, the 2D model finds the eigenvectors  $v_{1,2} = (k,1)$ , as defined in Eq. 10, where:

$$k = \frac{-s}{2} \pm \frac{\sqrt{B^2-4}}{2s \sin \alpha}, \quad B=(2 \cos \alpha - s \sin \alpha), \text{ and } \theta \text{ can be found from the dot product of } v \text{ with the x-axis:}$$

$$\cos \theta = k / \sqrt{(k^2+1)} \quad (14)$$

These four models are plotted in Fig. 9, along with the experimentally measured data points from *OR S*. Although the data points are scattered, there is a systematic trend that shows a clear correlation between  $\theta$  and  $\alpha$ . This trend is nearly linear but presents an apparent curvature, as predicted by the three non-linear models. The error bars in  $\theta$  represent the experimental uncertainty of positioning the sample in the microscope. The error bars in  $\alpha$  are much smaller because they represent *relative* orientations of Ni and Ag for the same position of the sample in the microscope. From this graph, we can conclude that the data support the models based on edge-to-edge matching, whether it is in the 1D sense, as in the topological approach, or in the 2D eigenvector approach. However, the scatter in the data is too large to favor one model over the others.

From the superposition of the light and dark green lines in Fig. 9 it is apparent that the 1D edge-to-edge model and the topological model predict essentially the same interface. Both models refer to a reference state where terrace planes in Ni and Ag are placed in contact in a specific *OR T* near  $\theta = 0^\circ$  and *OR O* near  $\theta = 54.5^\circ$ . Thus the reference state must be switched from a Ni(111) to Ni(100) terrace about halfway across the graph. In contrast, the lattice correspondence that determines the transformation matrix in the 2D model applies to the entire range.

---

\* Note that the model discussed by Pond et al. [35] describes an invariant line strain, which is achieved by allowing the ratio of step heights to vary. For a constant step height ratio (1.16 for Ag(111) on Ni(111)), Eq. B.8 in [35] describes the strain compensation normal to the interface (edge-to-edge matching), even if it does not compensate for the strain parallel to the interface. It can be shown that without the invariant line constraint, the topological model predicts a relationship between  $\theta$  and  $\alpha$  that is essentially identical to that of the 2D model.

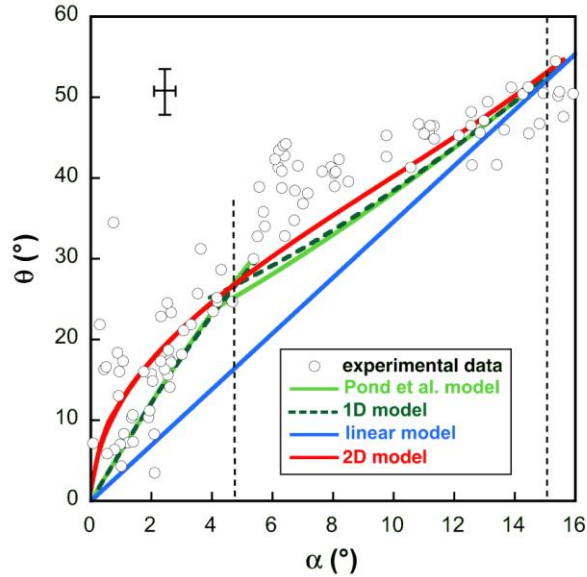


**Figure 9.** Plot of  $\theta$  versus  $\alpha$  comparing four models with the experimental data. The linear model is shown in blue (Eq. 11), the 2D model is shown in red (Eq. 14), the 1D edge-to-edge matching model is shown as a dark green dashed line (Eqs. 2 and 12) and the topological model is shown in light green (Eq. 13). The discontinuity around  $\theta = 25^\circ$  is due to the change of reference frames – from Ag(111) on Ni(111) (left) to Ag(111) on Ni(100) (right). The two thin dashed vertical lines indicate the positions of the invariant lines. The experimental data points were obtained by orientation imaging, using Euler angles to determine Ni(hkl) and Ag(HKL), finding  $\theta$  from the angle between Ni(hkl) and the nearest Ni(111), finding  $\phi$  from the angle between Ag(HKL) and the nearest Ag(111), and  $\alpha$  from  $\alpha = \phi - \theta$ . Error bars are indicated at top left.

The largest difference between the various models occurs in the low-angle regime, for  $\theta < 10^\circ$ . This is where the 2D model predicts  $\alpha = 0.7^\circ$ , the 1D model predicts  $\alpha = 1^\circ$ , and the linear model predicts  $\alpha = 3^\circ$ . Even within experimental error limits, these differences should be measurable. It will therefore be instructive to assess interfaces in this regime by high-resolution electron microscopy to ascertain their precise structure and ORs. A detailed examination of interfaces in this neighborhood is expected to reveal the distinction between the structures predicted by the different models.

The largest discrepancy between the data and the models appears in the middle of the range for  $\theta$  between 30 and 40°. In this range, the data points lie consistently above all the predictions. Experimental observations of interfaces in this range could shed light on a mechanism of accommodation that has not been considered in any of the models. This could include, for instance, periodic stacking faults, which in Ag bicrystals have been shown to lead to dissociated grain boundaries stabilized by the 9R phase [37].

#### **4.4. Comments on heteroepitaxy**

The conventional view on the heteroepitaxy of FCC films is that they either display  $\{111\}$  planes parallel to the substrate, or if the substrate is also FCC they tend to adopt *OR C*. Our studies of Ag ORs on more than two hundred Ni-substrate orientations [11] have shown a much more complex heteroepitaxial

system, even in this presumably simple FCC-on-FCC system. While it has been known for some time that Ag equilibrated on Ni(100) adopts a (111) interfacial orientation, i.e. the so-called oct-cube OR (*OR O*) [38], it has been shown more recently that this OR prevails in other FCC-on-FCC systems where the deposit possesses a lattice constant that is larger than that of the substrate by more than about 10% [34]. What our previous work [11,12,20] has uncovered is that there also exists an infinite set of "special" ORs (*OR S*) that develop as a transition from *OR T*, which prevails on Ni substrates oriented along the (111) to (210) line of the SST, to *OR O* at Ni(100).

The present paper has focused on the development of a model for relating the orientations of Ag to those of the Ni substrates in the regime of the "special" ORs. However, a classical axis-angle analysis of *OR S*, starting from a cube-on-cube reference and rotating about a common axis, as is usually performed for grain boundaries (e.g., [39]), does not lend itself to a simple interpretation. Except in the region of Ni(hkl) close to (100), such analyses yield a twin OR, within some apparent inaccuracy which can easily be attributed to experimental error. Only by going outside the description of ORs as disorientations and by using the twin correspondence as a reference does the simplicity of *OR S* as a systematic rotation around a common  $\langle 110 \rangle$  direction reveals itself. In this model we use linear interpolation to relate plane normals Ag(HKL) to Ni(hkl) and to obtain the corresponding OR via the rotation angle  $\alpha$ . The predictions of this linear model agree to within  $\sim 2^\circ$  with the experimental observations.

The second approach builds on the TLK model typically used in surface science. Ag films grow by atomic attachment at surface steps on terraces of the Ni substrate. The key role of  $\langle 110 \rangle$  step alignment in this system was emphasized in previous work [11,12]. Because terrace planes in Ag and Ni have different lattice spacings, the mismatch at each step can cause a small macroscopic rotation of the two lattices. This rotation increases as the step density increases with increasing inclination of the surface to the terrace planes. The same geometry may also be viewed as edge-to-edge matching of the terrace planes and can be described by either a moiré pattern in direct space or a  $\Delta\mathbf{g}$  vector in reciprocal space. However, this 1D model cannot explain why edge-to-edge matching does not lead to rotations in the *OR C* domain of the SST.

The third approach employs a 2D model generally used in phase transformations. It can be considered an extension of the edge-to-edge matching. Referred to the twin correspondence, the 2D transformation matrix can be written explicitly. *OR T* and *OR O* are both described by the same lattice correspondence and may be considered end-members of a continuous range of orientations (*OR S*). The range of possible orientations is given by the disappearance of eigenvectors at a critical rotation of  $20^\circ$  from *OR T*. The same criterion prohibits any rotation at all for the cube correspondence. This explains the difference between the two domains in the SST, characterized by *OR S* and *OR C*.

It is interesting to compare the interpretation of our results with some recent detailed X-ray diffraction measurements by Bellec et al. [15] of the OR adopted by Ag on a Ni(11 9 9) substrate. They find that Ag adopts a (9 9 7) orientation on the substrate, which corresponds to our angles  $\theta$  and  $\phi$  of  $5.6^\circ$  and  $6.5^\circ$ , respectively. For a Ni(11 9 9) substrate orientation, and with our Eq. 2, we compute an angle  $\phi$  of  $7.2^\circ$ , and

with our Eq. 6 we obtain  $\phi = 6.5^\circ$ . Thus, the agreement with those results is quite good. Bellec et al. also report that the FCC stacking of the Ag layer is reversed compared to that of the Ni substrate, as would be expected for *OR T*.

It is also interesting to note that in the case of the heteroepitaxy of oxide films on oxide substrates, it has been found, for SnO<sub>2</sub> films on columbite, that there exist two distinct domains of columbite substrate orientation in the columbite SST, which accommodate two different polymorphs of SnO<sub>2</sub> [18]. This observation is similar to ours, even though we observe no change in *crystallographic structure* here between Ag in *OR S* and Ag in *OR C*. In the case of the oxides, it could be that a better interfacial accommodation of the two polymorphs determines their stabilization.

Finally, with the advent of EBSD, and its capacity for simplifying the ease of acquiring data over the complete ranges of substrate orientation, one may speculate that many more examples of such unexpected orientation relationships remain to be discovered.

## **5. SUMMARY**

This work builds on previous combinatorial observations of Ag films on Ni substrates of many different orientations, which identified two distinct ORs: the traditional cube-on-cube OR is seen on roughly half of all surface orientations, and a special OR on the other half. Remarkably, the special OR varies continuously and systematically, ranging from a twin relationship to the so-called oct-cube relationship.

The systematic nature of this variation becomes apparent only by going outside the traditional framework of disorientations and the standard stereographic triangle. Using the twin correspondence as a reference frame, the variable orientation can be described as a gradual rotation from  $\alpha=0$  to  $15.8^\circ$  around a common  $\langle 110 \rangle$  direction, which lies close to, but not always in, the interface.

We present explicit expressions for the lattice rotation and corresponding interface plane normals for the entire orientation space covered by the special OR. This expression is based on an extension of a linear interpolation approach previously used for surface orientations along a line in orientation space. In the framework of the terrace-ledge-kink model of surface science the role of steps for atomic attachment helps understand the alignment of a set of  $\langle 110 \rangle$  directions. This mechanism also implies a macroscopic lattice rotation due to the mismatch in the spacing of terrace planes between Ag and Ni. The rotation due to this mismatch leads to edge-to-edge matching of terrace planes across a vicinal interface. An extension of this 1D approach to 2D employs the transformation matrix typically used in phase transformations. This approach also explains why the OR varies systematically only for the twin correspondence but remains locked for the cube-on-cube correspondence.

## **Acknowledgements**

We are grateful to S. Lartigue for a critical reading of the manuscript and many helpful comments. DC wishes to thank the Agence Nationale de la Recherche for support of her research under grant ANR-GIBBS-15-CE30-0016, and ADR thanks the Department of Energy for support under grant number DE-SC0019096.

## **Appendix A. Example of calculation of Ag(HKL) from Ni(hkl) for OR (S)**

For a given Ni(hkl) in the left half of the SST, the rotation angle  $\alpha$  can be found from Eq. 5 and the corresponding Ag(HKL) may be obtained from Eq. 3. As an example, take Ni(hkl) = (25 7 2). For this pole, a rotation angle of  $\alpha = 7.9^\circ$  is obtained from Eq. 5. Using the rotation matrix  $R(\beta)$  with  $\beta=70.5^\circ-7.9^\circ$ , we obtain Ag(HKL)=(0.586, 0.779, -0.225), when expressed as a unit vector. This is within  $1^\circ$  of the experimentally observed orientation of the Ag film: Ag(HKL)=(0.566, 0.793, -0.226).

**Appendix B. Relationship between moiré patterns, edge-to-edge plane matching and  $\Delta\mathbf{g}$  vectors**

The superposition of two sets of lattice planes of spacing  $d_1$  and  $d_2$ , rotated by an angle  $\alpha$  gives rise to moiré fringes, as shown in Fig. B1a. The corresponding diffraction vectors  $\mathbf{g}_1$ ,  $\mathbf{g}_2$  and  $\Delta\mathbf{g}$  are shown in Fig. B1b. The moiré fringes are normal to  $\Delta\mathbf{g}$  and their spacing is inversely proportional to  $|\Delta\mathbf{g}|$ . In Fig. B1c, an interface has been placed between the two lattices in a plane parallel to the moiré fringes, i.e. normal to  $\Delta\mathbf{g}$ . It is apparent that in such an interface the corresponding planes meet edge-to-edge. This simple geometrical tool greatly simplifies the analysis of small rotations or changes in lattice parameter. In particular, it allows representation of the lattice rotation necessary for vicinal surfaces, where a small difference in lattice spacing of the terrace planes must be accommodated at steps. As the substrate vicinal surface rotates by an angle  $\theta$ , the two lattices must rotate by a relative angle  $\alpha$ , if the terrace planes are to meet edge-to-edge in the interface (see Eq. 6).

The reciprocal space analysis shown in Fig. B1 for the 1D case of a single set of corresponding planes can be extended to the 2D case of a transformation between two lattices. This has been discussed in some detail in the context of optimal interfaces between two dissimilar lattices [5-9,22-25,33,40].

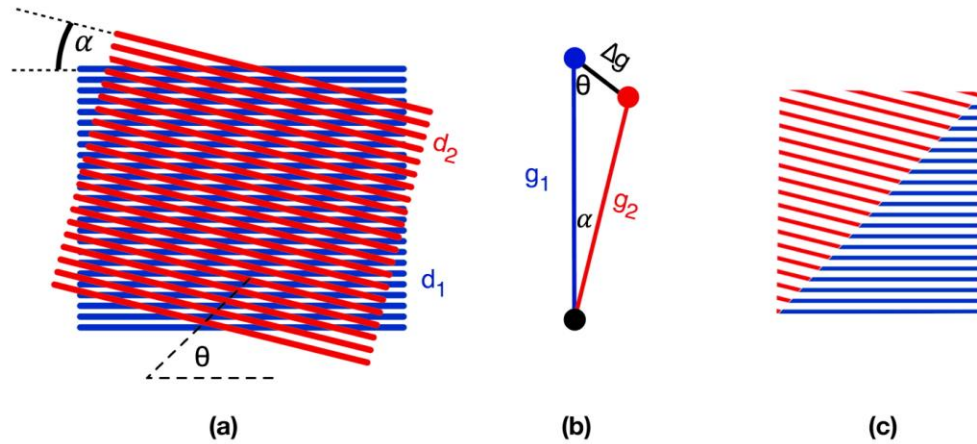


**Figure B1.** Representation in direct and reciprocal space of the relationship between lattice rotation, interface plane and edge-to-edge plane matching; a) moiré pattern generated by superposition of two lattices with spacings  $d_1$  and  $d_2$  rotated through an angle  $\alpha$ ; b) reciprocal space representation of the direct-space geometry in a), with  $\mathbf{g}$ -vectors perpendicular to the corresponding planes; c) the two lattices are drawn meeting in an interface parallel to the moiré fringes to show that for this interface, the two planes meet edge-to-edge. Note that the difference vector  $\Delta\mathbf{g} = \mathbf{g}_2 - \mathbf{g}_1$  lies perpendicular to the interface plane, at an angle  $\theta$  to  $\mathbf{g}_1$  [5-9,22-25,33,40].

## **REFERENCES**

- [1] A.P. Sutton, R.W. Balluffi, *Interfaces in crystalline materials*, Oxford University Press, Oxford, 1995.
- [2] J.M. Howe, *Interfaces in Materials: Atomic structure, kinetics and thermodynamics of solid–vapor, solid–liquid and solid–solid Interfaces*, John Wiley & Sons, New York, 1997.
- [3] J.M. Howe, *Structure, composition and energy of solid–solid interfaces*, 5th ed., Elsevier B.V, 2014, pp. 1317-1451.
- [4] J.W. Christian, *The theory of transformation in metals and alloys*, Pergamon Press, 1975.
- [5] W.Z. Zhang, G.C. Weatherly, On the crystallography of precipitation, *Prog. Mater. Sci.* 50 (2005) 181-292.
- [6] J.F. Nie, Crystallography and migration mechanisms of planar interphase boundaries, *Acta Mater.* 52 (2004) 795-807.
- [7] M.W.H. Braun, J.H. Van Der Merwe, Reciprocal-space formulation and prediction of misfit accommodation in rigid and strained epitaxial systems, *Metall. Mater. Trans. A* 33 (2002) 2485-2494.
- [8] M.X. Zhang, P.M. Kelly, Crystallographic features of phase transformations in solids, *Prog. Mater. Sci.* 54 (2009) 1101-1170.
- [9] U. Dahmen, Orientation relationships in precipitation systems, *Acta Metall.* 30 (1982) 63-73.
- [10] G.S. Rohrer, Grain boundary energy anisotropy: a review, *J. Mater. Sci.* 46 (2011) 5881–5895.
- [11] D. Chatain, P. Wynblatt, A.D. Rollett, G.S. Rohrer, Importance of interfacial step alignment in hetero-epitaxy and orientation relationships: the case of Ag equilibrated on Ni substrates. Part 2 experiments, *J. Mater. Sci.* 50 (2015) 5276-5285.
- [12] P. Wynblatt, D. Chatain, Importance of interfacial step alignment in hetero-epitaxy and orientation relationships: the case of Ag equilibrated on Ni substrates. Part 1 computer simulations, *J. Mater. Sci.* 50 (2015) 5262-5275.
- [13] F.C. Frank, Martensite, *Acta Metall.* 1 (1953) 15-21.
- [14] Y. Garreau, A. Coati, A. Zobelli, J. Creuze, "Magic" heteroepitaxial growth on vicinal surfaces, *Phys. Rev. Lett.* 91 (2003) 116101.
- [15] A. Bellec, Y. Garreau, J. Creuze, A. Vlad, F. Picca, M. Sauvage-Simkin, A. Coati, Ag on a Ni vicinal surface: Coupling Stranski-Krastanov and "magic" heteroepitaxial growth, *Phys. Rev. B* 96 (2017) 085414.
- [16] Y. Zhang, A.M. Schultz, L. Li, H. Chien, P.A. Salvador, G.S. Rohrer, Combinatorial substrate epitaxy: A high-throughput method for determining phase and orientation relationships and its application to BiFeO<sub>3</sub>/TiO<sub>2</sub> heterostructures, *Acta Mater.* 60 (2012) 6486-6493.
- [17] N.V. Burbure, P.A. Salvador, G.S. Rohrer, Orientation and phase relationships between titania films and polycrystalline BaTiO<sub>3</sub> substrates as determined by electron backscatter diffraction mapping, *J. Am. Ceram. Soc.* 93 (2010) 2530-2533.
- [18] J. Wittkamper, Z. Xu, B. Kombaiah, F. Ram, M. De Graef, J.R. Kitchin, G.S. Rohrer, P.A. Salvador, Competitive growth of scrutinyite ( $\alpha$ -PbO<sub>2</sub>) and rutile polymorphs of SnO<sub>2</sub> on all orientations of columbite CoNb<sub>2</sub>O<sub>6</sub> substrates, *Cryst. Growth & Des.* 17 (2017) 3929-3939.
- [19] S.M. Foiles, M.I. Baskes, M.S. Daw, Embedded-atom-method functions for the FCC metals Cu, Ag, Au, Ni, Pd, Pt, and their alloys, *Phys. Rev. B* 33 (1986) 7983-7991.
- [20] P. Wynblatt, D. Chatain, Two-dimensional versus three-dimensional constraints in hetero-epitaxy/orientation relationships, *J. Mater. Sci.* 52 (2017) 9630-9639.
- [21] R.C. Pond, D.L. Medlin, A. Serra, A study of the accommodation of coherency strain by interfacial defects at a grain boundary in gold, *Philos. Mag.* 86 (2006) 4667-4684.
- [22] G.S. Rohrer, *Structure and bonding in crystalline materials*, Cambridge University Press, Cambridge, 2001.
- [23] P.M. Kelly, M.X. Zhang, Edge-to-edge matching-the fundamentals, *Metall. Mater. Trans. A* 37 (2006) 833-839.

- [24] W.Z. Zhang, G.R. Purdy, O-lattice analyses of interfacial misfit. I. General considerations, *Philos. Mag. A* 68 (1993) 279-290.
- [25] W.Z. Zhang, G.R. Purdy, O-lattice analyses of interfacial misfit. II. Systems containing invariant lines, *Philos. Mag. A* 68 (1993) 291-303.
- [26] U. Dahmen, Split reflections from broken mirrors: Symmetry-breaking in the making of materials microstructures, in: K.M. Krishnan (Ed.), *Microstructures of Materials*, San Francisco Press, 1992, pp. 6-11, also internal LBL report #33474.
- [27] I.N. Stranski, Zur Theorie des Kristallwachstums, *Z. Phys. Chem.* 136 (1928) 259-278.
- [28] M.A. Van Hove, G.A. Somorjai, A new microfacet notation for high-Miller-index surfaces of cubic materials with terrace, step and kink structures, *Surf. Sci.* 92 (1980) 489-518.
- [29] R.V. Zucker, D. Chatain, U. Dahmen, S. Hagège, W.C. Carter, New software tools for the calculation and display of isolated and attached interfacial-energy minimizing particle shapes, *J. Mater. Sci.* 47 (2012) 8290-8302.
- [30] A. Kelly, G.W. Groves, P. Kidd, *Crystallography and crystal defects*, Revised Edition, John Wiley & Sons, New York, 2000.
- [31] S.Q. Xiao, J.M. Howe, Analysis of a two-dimensional invariant line interface for the case of a general transformation strain and application to thin-film interfaces, *Acta Mater.* 48 (2000) 3253-3260.
- [32] J.W. Christian, Lattice correspondence, atomic site correspondence and shape change in "diffusional-displacive" phase transformations, 42 (1997) 101-108.
- [33] U. Dahmen, A comparison between three simple crystallographic principles of precipitate morphology, *Metall. Mater. Trans. A* 25 (1994) 1857-1863.
- [34] P.Y. Hsiao, Z.H. Tsai, J.H. Huang, G.P. Yu, Strong asymmetric effect of lattice mismatch on epilayer structure in thin film deposition, *Phys. Rev. B* 79 (2009) 155414.
- [35] R.C. Pond, S. Celotto, J.P. Hirth, A comparison of the phenomenological theory of martensitic transformations with a model based on interfacial defects, *Acta Materialia*. 51 (2003) 5385-5398.
- [36] C.M. Wayman, *Introduction to the Crystallography of Martensitic Transformations*, Macmillan, New York, 1964.
- [37] F. Ernst, M.W. Finnis, D. Hofmann, T. Muschik, U. Schonberger, U. Wolf, M. Methfessel, Theoretical prediction and direct observation of the 9R structure in Ag, *Phys. Rev. Lett.* 69 (1992) 620-623.
- [38] Y. Gao, P.G. Shewmon, S.A. Dregia, Investigation of low-energy interphase boundaries in Ag/Ni by computer simulation and crystallite rotation, *Acta Metall.* 37 (1989) 3165-3175.
- [39] D. Wolf, Atomic-level geometry of crystalline interfaces, in: D. Wolf, S. Yip (Eds.), *Materials Interfaces*, Chapman & Hall, London, 1992, pp 1-57.
- [40] A.R.S. Gautam, J.M. Howe, A method to predict the orientation relationship, interface planes and morphology between a crystalline precipitate and matrix: part II - application, *Philos. Mag.* 93 (2013) 3472-3490.